FRAGILE X SYNDROME

Reducing eIF4E-eIF4G interactions restores the balance between protein synthesis and actin dynamics in fragile X syndrome model mice

Emanuela Santini,[1,2]* Thu N. Huynh,[1†‡] Francesco Longo,[1‡] So Yeon Koo,[1] Edward Mojica,[1] Laura D'Andrea,[3] Claudia Bagni,[3,4,5,6] Eric Klann[1§]

Fragile X syndrome (FXS) is the most common form of inherited intellectual disability and autism spectrum disorder. FXS is caused by silencing of the *FMR1* gene, which encodes fragile X mental retardation protein (FMRP), an mRNA-binding protein that represses the translation of its target mRNAs. One mechanism by which FMRP represses translation is through its association with cytoplasmic FMRP-interacting protein 1 (CYFIP1), which subsequently sequesters and inhibits eukaryotic initiation factor 4E (eIF4E). CYFIP1 shuttles between the FMRP-eIF4E complex and the Rac1–Wave regulatory complex, thereby connecting translational regulation to actin dynamics and dendritic spine morphology, which are dysregulated in FXS model mice that lack FMRP. Treating FXS mice with 4EGI-1, which blocks interactions between eIF4E and eIF4G, a critical interaction partner for translational initiation, reversed defects in hippocampus-dependent memory and spine morphology. We also found that 4EGI-1 normalized the phenotypes of enhanced metabotropic glutamate receptor (mGluR)–mediated long-term depression (LTD), enhanced Rac1–p21-activated kinase (PAK)–cofilin signaling, altered actin dynamics, and dysregulated CYFIP1/eIF4E and CYFIP1/Rac1 interactions in FXS mice. Our findings are consistent with the idea that an imbalance in protein synthesis and actin dynamics contributes to pathophysiology in FXS mice, and suggest that targeting eIF4E may be a strategy for treating FXS.

INTRODUCTION

Fragile X syndrome (FXS) is the most commonly inherited form of intellectual disability (ID) and autism spectrum disorder (ASD) (*1*). FXS is typically caused by transcriptional silencing of the X-linked *fragile X mental retardation 1* (*FMR1*) gene and results in the loss of the encoded protein product, fragile X mental retardation protein (FMRP), an mRNA-binding protein (*2*–*4*) that regulates dendritic transport (*5*) and controls the translational repression of specific mRNAs (*2*, *6*). In the absence of FMRP, it is believed that many mRNA targets are up-regulated (*6*), resulting in increased protein synthesis in the brain (*7*). One translation-repressing function of FMRP is achieved with the assistance of the cytoplasmic FMRP-interacting protein 1 (CYFIP1), which sequesters the cap-binding eukaryotic initiation factor 4E (eIF4E) and thereby prevents the initiation of translation of specific mRNAs tethered to FMRP (*8*, *9*).

eIF4E binds to the m^7G cap structure at the 5′ terminus of mRNA and is involved in regulating the initiation step of protein synthesis (*10*). When eIF4E binds to the eIF4G, other initiation factors and ribosomal proteins are recruited to the mRNA so that protein synthesis can begin. eIF4E is tightly regulated by signaling pathways mediated by the mechanistic target of rapamycin complex 1 (mTORC1) and extracellular signal–regulated kinase (ERK). 4E-binding proteins (4E-BPs), such as brain-enriched 4E-BP2, CYFIP1, and neuroguidin, control the association of eIF4E with eIF4G by binding and inhibiting eIF4E (*9*–*15*). Upon activation, mTORC1 phosphorylates and inhibits 4E-BP2, thereby releasing eIF4E so that it can bind to eIF4G (*11*–*13*, *16*–*18*). The ERK signaling pathway also controls translation initiation via phosphorylation of eIF4E by the kinases MNK1 and MNK2, which is believed to facilitate the formation of the translation initiation complex (*19*–*21*).

FMRP and mRNAs are localized in dendritic spines (*22*), and the FMRP-CYFIP1-eIF4E inhibitory complex ensures an appropriate rate of local protein synthesis in response to synaptic activity, which is fundamental for triggering multiple forms of long-term synaptic plasticity at glutamatergic synapses, including long-term potentiation (LTP) and metabotropic glutamate receptor (mGluR)–dependent long-term depression (LTD) (*3*, *23*, *24*). Accordingly, mouse models of FXS are characterized by widespread alterations in synaptic plasticity (*3*, *25*, *26*), dysregulated mRNA translation, and aberrant forms of LTP and LTD in cortex and hippocampus (*27*–*29*). Particularly important for FXS are group 1 mGluRs, which trigger protein synthesis resulting in LTD at glutamatergic synapses in hippocampal area CA1 (*30*–*34*). On the basis of the finding that mGluR-LTD is exaggerated in the hippocampus of FXS model mice (*27*), it was proposed that the lack of FMRP results in exaggerated translation of synaptic plasticity–related mRNAs downstream of group 1 mGluR activation (*35*). In addition, enhanced protein synthesis observed in the brains of FXS model mice is occluded by stimulation of group 1 mGluRs but is normalized by inhibition of the same class of receptors (*7*, *36*, *37*). mTORC1, ERK signaling, and an increase in association of eIF4E with eIF4G in the eIF4F initiation complex are enhanced in the hippocampus of FXS model mice (*38*–*40*). Moreover, inhibition of components of the mTORC1 and ERK signaling pathways that couple mGluRs to protein synthesis normalizes aberrant phenotypes in FXS model mice (*38*, *39*, *41*–*46*).

[1]Center for Neural Science, New York University, New York, NY 10003, USA. [2]Department of Neurology, Columbia University, New York, NY 10032, USA. [3]Department of Biomedicine and Prevention, University of Rome "Tor Vergata," 00133 Rome, Italy. [4]Center for Human Genetics and Leuven Research Institute for Neuroscience and Disease, KU Leuven, 3000 Leuven, Belgium. [5]VIB Center for the Biology of Disease, 3000 Leuven, Belgium. [6]Department of Fundamental Neuroscience, University of Lausanne, 1005 Lausanne, Switzerland.
*Present address: Department of Neurology, Columbia University, New York, NY 10032, USA.
†Present address: Brain and Mind Research Institute and Department of Psychiatry, Weill Cornell Medical College, New York, NY 10065, USA.
‡These authors contributed equally to this work.
§Corresponding author. Email: eklann@cns.nyu.edu

Finally, either genetic deletion of 4E-BP2 (*47*) or overexpression of eIF4E (*48*) generates ASD-like behaviors and altered synaptic function in mice similar to those displayed by FXS model mice, suggesting that dysregulation of signaling pathways that regulate protein synthesis is a common pathogenic pathway involved in both FXS and ASD (*49*, *50*).

Structural changes in dendritic spine morphology are important for synaptic plasticity, and the signaling pathways that control actin dynamics are involved in the reorganization of spine cytoskeleton occurring during long-lasting forms of synaptic plasticity (*51*–*54*). One of the more striking phenotypes described in both FXS model mice and FXS patients are changes in dendritic spine morphology, which are characterized by increased numbers of long, thin dendritic spines relative to the more mature mushroom-shaped spines (*55*, *56*). This observation suggests that the absence of FMRP disturbs the cytoskeletal machinery responsible for the structural and synaptic plasticity of dendritic spines.

The Rho family of small guanosine triphosphatases (GTPases), including Rac1, are signaling molecules that regulate actin dynamics in response to synaptic activity (*57*–*60*). Rac1 cycles between an inactive guanosine diphosphate (GDP)–bound and an active guanosine triphosphate (GTP)–bound conformations controlled by the catalytic activity of guanine exchange factors (GEFs) and GTPase activating proteins (GAPs), respectively (*61*). Rac1 signaling pathway has been implicated in learning and memory and in X-linked ID, which is also characterized by abnormalities in dendritic spine morphology (*54*, *62*). Active Rac1 regulates actin dynamics by activating Rho-associated kinases (ROCK), such as p21-activated kinases (PAKs) (*63*), which, in turn, determine the phosphorylation of cofilin at Ser^3 via activity of LIM motif-containing protein kinases 1 and 2 (LIMK1/2) (*64*, *65*). Cofilin is an actin-binding protein that regulates actin turnover, and its dephosphorylation leads to polymerization and stabilization of actin filaments, and suppresses actin turnover (*66*). Accumulating evidence suggests a link between the Rac1-PAK pathway and FMRP. In *Drosophila*, orthologs of *Rac1* and *Fmr1* are genetically linked (*67*). In murine fibroblasts, FMRP is connected to Rac1 and the actin remodeling functions of Rac1 are altered in the absence of FMRP (*68*), and activation of Rac1-PAK pathway induced by synaptic activity is defective in FXS model mice (*54*). Notably, structural, synaptic, and behavioral phenotypes displayed by FXS model mice are rescued either by genetically expressing a dominant-negative form of PAK or by pharmacological blockade of PAK (*69*–*71*).

Active Rac1-GTP also regulates actin dynamics by recruiting CYFIP1 to the Wave regulatory complex (WRC) (*67*, *72*). On the basis of this observation, it was proposed that CYFIP1 is associated with two distinct protein complexes: FMRP-CYFIP1-eIF4E, which represses translation of specific mRNAs, and Rac1-WRC, which regulates actin dynamics (*73*). Synaptic activity changes the equilibrium of CYFIP1 between the two complexes and promotes protein synthesis as well as morphological and synaptic plasticity (*67*, *72*, *74*).

Here, we show that inhibiting the association of eIF4E to eIF4G with 4EGI-1 (*48*, *75*, *76*) reverses memory deficits and altered dendritic morphology in the hippocampus of FXS model mice. In addition, we show that the Rac1-PAK pathway is activated downstream of mGluRs and is defective in hippocampal area CA1 of FXS model mice. Treatment of hippocampal slices with 4EGI-1 creates free eIF4E that can compete with Rac1-GTP for the binding of CYFIP1. Thus, in the presence of 4EGI-1, abundance of the FMRP-CYFIP1-eIF4E complex increases, whereas that of the CYFIP1-Rac1-GTP-WRC complex decreases. Furthermore, the decrease of CYFIP1-Rac1-GTP reduces the overactivation of Rac1-PAK-cofilin signaling in FXS model mice. Thus, restoring the balance between signaling pathways that regulate protein synthesis and actin dynamics normalizes hippocampal phenotypes in FXS model mice.

RESULTS

Inhibition of eIF4E-eIF4G interactions normalizes cognitive impairments and spine morphology in FXS model mice

FXS model mice are characterized by an increased association of eIF4E with eIF4G, exaggerated net protein synthesis, ASD-like behaviors, and altered synaptic function (*38*–*41*) that are similar to ASD mouse models with either genetic deletion of 4E-BP2 (*47*) or overexpression of eIF4E (*48*). Because administration of 4EGI-1, which inhibits eIF4E-eIF4G interactions, rescues multiple ASD-like phenotypes in 4E-BP2 knockout and eIF4E transgenic mice (*47*, *48*), we asked whether 4EGI-1 had similar effects in FXS model mice.

FXS model mice exhibit impairments in specific learning and memory tasks such as context discrimination (*77*, *78*). Context discrimination is a hippocampus-dependent form of associative learning in which mice are trained to discriminate between two environments, one in which they receive a shock (S+) and the other in which they do not (S−). The chambers have both unique and shared cues (*79*, *80*). In this test, a discrimination ratio was calculated using the percentage of time spent freezing in the neutral context (S−) divided by the percentage of time spent freezing in the shock-paired context (S+). We first trained FXS model mice and their wild-type littermates in the two contexts on day 1. During the acquisition phase of the task, all the mice displayed a discrimination ratio close to zero irrespective of their genotypes or treatments (Fig. 1A). This result suggests that the two contexts (S+ and S−) are not intrinsically aversive to the mice. The following day (day 2), we performed the context discrimination test after 4EGI-1 was infused into the lateral ventricle of the mice at a dose (100 μM) previously used in experiments of auditory threat conditioning (*81*). One hour after infusion of either 4EGI-1 or vehicle, we placed the mice in the S− context and then the S+ context after a 1.5-hour intertrial interval. We found that FXS model mice displayed an increased discrimination ratio, resulting from higher freezing behavior in the S− context relative to wild-type mice (Fig. 1B), which indicates that the FXS mice have impairments in the ability to discriminate between the S+ and S− contexts. Infusion of 4EGI-1 significantly attenuated the impairment in context discrimination in FXS mice (Fig. 1B). In contrast, wild-type mice were able to discriminate between the two contexts regardless of drug treatment (Fig. 1B). These results indicate that FXS model mice are impaired in context discrimination, which is normalized by 4EGI-1.

Another phenotype shared by FXS, eIF4E transgenic, 4E-BP2 knockout mice, as well as FXS and ASD patients, is altered dendritic spine density and morphology (*55*, *56*). Because abnormal spine density is normalized in FXS model mice by inhibiting upstream modulators of eIF4E (*39*), we proceeded to determine whether 4EGI-1 could also normalize the increased density of dendritic spines previously described in the hippocampus of FXS model mice (*55*, *56*). We infused either 4EGI-1 or vehicle into the ventricles of wild-type and FXS model mice and performed Golgi staining on the brains 24 hours later. We measured the spine density from primary apical dendrites in stratum radiatum of area CA1 of the hippocampus. We found that there was a significant difference between genotype and drug treatment (Fig. 1, C and D). Specifically, there was a significant increase

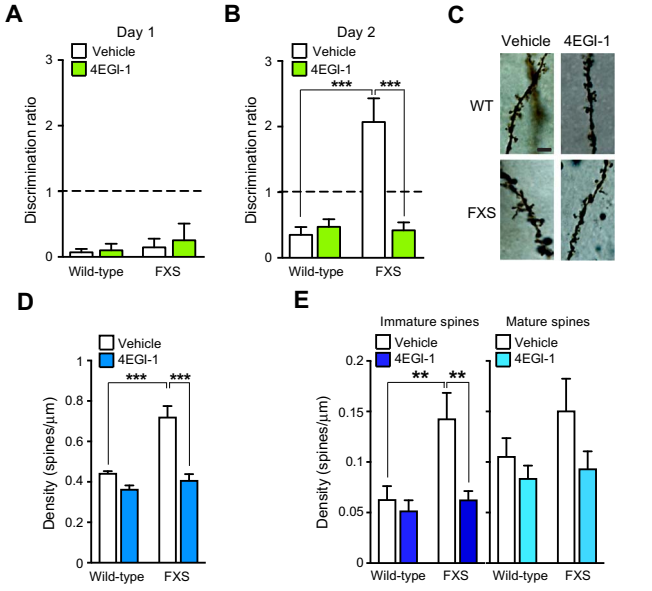

Fig. 1. Inhibition of eIF4E-eIF4G interactions restores deficits in context discrimination and increases spine density in FXS model mice. (**A** and **B**) Mean discrimination ratio [percentage of time spent in freezing behavior in the unpaired (S−) divided by the paired (S+) context] of FXS model mice and wild-type (WT) littermates in the context discrimination test, performed on day 1 during the acquisition phase of the test (A) and on day 2 performed 1 hour after intracerebroventricular infusions of 4EGI-1 (B; 100 μM). n = 10 to 12 mice per treatment; comparisons of genotype ($F_{1,39}$ = 15.35), treatment ($F_{1,39}$ = 12.94), and time × treatment interaction ($F_{1,39}$ = 17.39) were significantly different by two-way analysis of variance (ANOVA), each ***P < 0.005; ***P < 0.005 by Tukey's multiple comparisons test. (**C**) Representative images of the dendritic spines of CA1 hippocampal neurons in WT and FXS model mice treated with vehicle or 4EGI-1 (100 μM infused in the lateral ventricles 24 hours before Golgi staining). n = 15 to 20 neurons per mouse; 3 to 4 mice per genotype per treatment. Scale bar, 3 μm. (**D**) Density of total spines in mice described in (C). Comparisons of genotype ($F_{1,11}$ = 21.48), treatment ($F_{1,11}$ = 31.92) (each ***P < 0.005), and time × treatment interaction ($F_{1,11}$ = 11.38) (**P < 0.01) were significantly different by two-way ANOVA; ***P < 0.005 by Tukey's multiple comparisons test. (**E**) Analysis of spine density in mice described in (C), distinguishing immature (filopodia and thin) and mature (stubby, mushroom, and branched) spines. For the immature spine densities, comparisons of genotype ($F_{1,26}$ = 7.37), treatment ($F_{1,26}$ = 7.5), and time × treatment interaction ($F_{1,26}$ = 4.3) were significantly different by two-way ANOVA, each *P < 0.05; **P < 0.01 by Tukey's multiple comparisons test. Difference among mature spine densities was not significant by two-way ANOVA.

in spine density in FXS model mice compared to wild-type littermates. In contrast, there was no difference between wild-type mice treated with vehicle and FXS model mice treated with 4EGI-1, indicating that 4EGI-1 normalized the increased spine density present in FXS model mice. Moreover, there was no significant difference in spine density between wild-type mice treated with either vehicle or 4EGI-1, indicating that 4EGI-1 does not markedly alter spine density in wild-type mice (Fig. 1, C and D). In addition, we analyzed two morphological classes of spines, namely, mature (which included stubby, mushroom, and branched spines) and immature (which included filopodia and long thin spines) (Fig. 1E). The density of immature spines was significantly increased in FXS model mice and was normalized (restored to wild-type levels) by 4EGI-1 treatment. In contrast, the density of mature spines was not significantly different between either genotypes or treatments, although there was a trend for 4EGI-1 to reduce mature spine density in FXS mice (Fig. 1E). These results indicate that FXS model mice display increased density of specifically immature spines and that 4EGI-1 normalizes this increase (Fig. 1, C to E).

4EGI-1 normalizes increased mGluR-LTD in FXS model mice

Consistent with the increase in eIF4E-eIF4G interaction, basal protein synthesis is increased and mGluR-dependent LTD is enhanced in FXS model mice, suggesting that many of the phenotypes displayed in FXS model mice are because of excessive protein synthesis downstream of group 1 mGluRs (*7*, *27*, *35*, *36*). We recorded field excitatory postsynaptic potentials (fEPSPs) in the stratum radiatum of CA1 hippocampal neurons in response to Schaffer collateral stimulation and induced mGluR-LTD by applying 3,5-dihydroxyphenylglicine (DHPG; 10 min, 50 μM), an agonist of group 1 mGluRs, either with or without 4EGI-1 (preincubated for at least 40 min, 100 μM). In agreement with previous studies, we observed similar baseline synaptic transmission between hippocampal slices obtained from wild-type and FXS model mice (Fig. 2, A to C) but enhanced mGluR-LTD (induced by application of DHPG; 50 μM for 10 min) in hippocampal area CA1 of slices from FXS model mice (Fig. 2, A, B, and D). Notably, application of 4EGI-1 (100 μM for at least 40 min before the start of the recordings) significantly reduced mGluR-LTD in FXS model mice (Fig. 2, B and D). Application of 4EGI-1 did not alter mGluR-LTD in wild-type mice (Fig. 2, A and D). This finding is consistent with similar observations from mGluR-LTD experiments performed in the presence of cercosporamide, an inhibitor of eIF4E phosphorylation, in wild-type and FXS model mice (*39*). These experiments suggest that altered eIF4E function is involved in the expression of enhanced mGluR-LTD in FXS model mice but that it is not sufficient for mGluR-LTD in wild-type mice.

In contrast to wild-type mice, hippocampal mGluR-LTD in FXS model mice is insensitive to general protein synthesis inhibitors (*27*, *38*, *82*, *83*). Therefore, we asked whether the normalized mGluR-LTD in slices from FXS mice treated with 4EGI-1 was sensitive to the general protein synthesis inhibitor anisomycin. Toward this end, we incubated hippocampal slices obtained from wild-type and FXS model mice with anisomycin (20 μM) and 4EGI-1 (100 μM) and induced mGluR-LTD. Concomitant application of anisomycin with 4EGI-1 blocked mGluR-LTD in wild-type slices (Fig. 2, A and D), consistent with previous results (*27*, *38*). In contrast, coapplication of anisomycin and 4EGI-1 did not significantly alter the effects of 4EGI-1 alone on mGluR-LTD in slices from FXS model mice (Fig. 2, B and D), suggesting that LTD is sensitive to targeted eIF4E/cap-dependent translation inhibitors and insensitive to general protein synthesis inhibitors. Because general protein synthesis inhibitors such as anisomycin block both cap-dependent and cap-independent protein synthesis, our result indicates that mGluR-LTD in FXS is still independent on protein synthesis and that the mechanism of action of 4EGI-1 may affect simultaneously other signaling pathway(s) (that is, actin dynamics). Application of 4EGI-1 alone or with anisomycin did not alter baseline synaptic transmission in either wild-type or FXS model mice (Fig. 2C). These results indicate that inhibition of eIF4E-eIF4G interactions in FXS model mice reduces enhanced mGluR-LTD via a molecular mechanism independent of protein synthesis.

Rac1 signaling and actin dynamics are altered in FXS model mice

In addition to binding eIF4G to form the initiation complex, eIF4E also binds CYFIP1, which shuttles between the translation repressor FMRP and the WRC, where it is recruited by active (GTP-loaded)

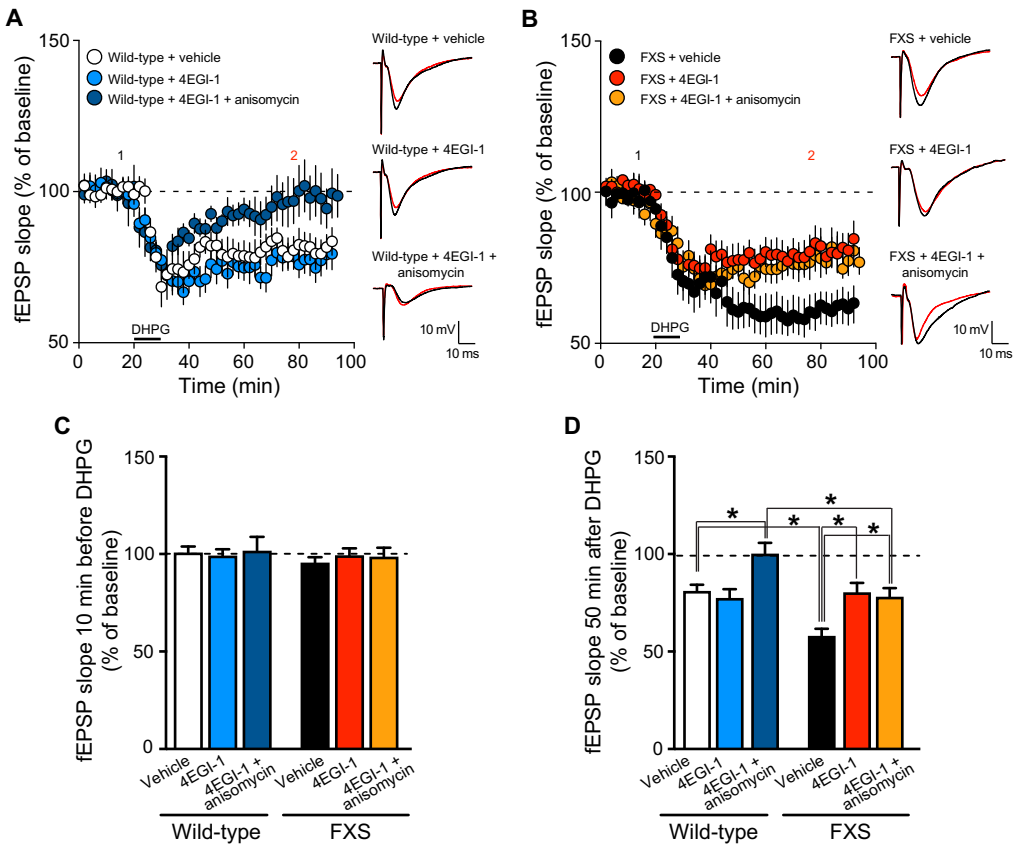

Fig. 2. Inhibition of eIF4E-eIF4G interactions normalizes mGluR-LTD independently of protein synthesis in FXS model mice. (**A** and **B**) mGluR-LTD experiments in hippocampal slices from WT (A) and FXS model (B) mice. mGluR-LTD was elicited by application of DHPG (50 μM; 10 min) 20 min after stable baseline recordings, performed in the presence or absence of 4EGI-1 (100 μM; applied at least 40 min before DHPG) alone or with anisomycin (20 μM; applied at least 10 min before DHPG). Both drugs were present in the perfusion bath until the end of the recordings. mGluR-LTD in slices from WT mice. $n = 7$ to 12 (WT) or 9 to 13 (FXS) slices per treatment. Representative fEPSPs of baseline (black; assessed before DHPG, denoted by 1 in the graph) and mGluR-LTD (red; assessed after DHPG, denoted by 2 in the graph) are shown on the right of each graph. (**C** and **D**) Average mGluR-LTD in slices described in (A) and (B), 10 min before (C) or 50 min after (D) DHPG application. n =7 to 13 slices per genotype per treatment. (C) Not significantly different by two-way ANOVA. (D) Comparisons of treatment ($F_{2,51} = 7.83$), genotype ($F_{2,51} = 11.81$) (each $^{**}P < 0.01$), and treatment × genotype interaction ($F_{2,51} = 4.32$) ($^{*}P < 0.05$) were significantly different by two-way ANOVA; $^{*}P < 0.05$ by Tukey's multiple comparisons test. Data are means ± SEM normalized to WT controls.

Rac1 (*9*, *67*, *72*). In the absence of FMRP, both eIF4E-binding dynamics and Rac1-actin remodeling functions are altered in murine fibroblasts (*9*, *68*), and the gene orthologs of *Rac1* (*dRac1*) and *Fmr1* (*dFmr1*) are genetically linked in *Drosophila* (*67*). For example, aberrant eye morphology observed in flies overexpressing *dFmr1* is enhanced by *dRac1* overexpression and suppressed by reduced *dRac1* expression (*67*). Moreover, Rac1 has been implicated in the etiology of FXS (*67*, *72*, *74*). For example, Rac1 abundance is increased in the brains of FXS patients, suggesting that *RAC1* mRNA expression is repressed by FMRP (*84*). Thus, we asked whether Rac1 levels were altered in FXS model mice. Western blot analyses of the hippocampal CA1 region of 3- to 6-week-old mice revealed no significant difference in Rac1 abundance between FXS model mice and their wild-type littermates (Fig. 3A). However, using a PAK pull-down assay consisting of a glutathione agarose matrix fused to the p21-binding domain (PBD) of PAK, which specifically binds the active form of Rho-GTPases (see Materials and Methods), we found increased Rac1-GTPase activity in the FXS model mice (Fig. 3B), indicating that baseline activation, albeit not protein abundance, of Rac1 is increased in FXS model mice.

Rac1 is a Rho-GTPase that regulates actin dynamics at synapses by controlling the activation of PAK1/2 (*57*, *85*). PAK1/2 may be involved in FXS pathology, given that pharmacological (*71*) and genetic (*70*) inhibition of PAKs alleviates multiple phenotypes in FXS model mice. Thus, we asked whether PAK1/2 signaling downstream of Rac1-GTP is increased in FXS model mice. Western blot analyses revealed increased phosphorylation of PAK1/2 at $Ser^{199/204}$ and $Ser^{192/197}$ (Fig. 3C). This increased phosphorylation was accompanied by increased phosphorylation of cofilin at Ser^{3} in the FXS model mice (Fig. 3D). We found no difference in total abundances of PAK1/2, cofilin, and tubulin between wild-type and FXS mice (Fig. 3, E to G). These results indicate that Rac1-PAK1/2-cofilin signaling activity is altered in the hippocampal area CA1 of FXS model mice.

Increased phosphorylation of PAK1/2 and cofilin affects actin polymerization (*51*, *57*). Specifically, phosphorylation of actin-binding proteins, such as cofilin, inactivates actin turnover that results in enhanced polymerization and stabilization of actin filaments (*86*, *87*). Actin polymerization can be measured by analyzing the amount of monomeric globular actin (G-actin) and polymerized filamentous actin (F-actin) in cells and tissues. Because the transition between these two forms of actin is dynamic and controlled by synaptic activity (*51*, *57*), we analyzed the ratio of F-actin to G-actin in hippocampal area CA1 of FXS model mice and their wild-type littermates. We found that the ratio of F-actin to G-actin, which reflects the balance between actin polymerization and depolymerization, is increased in FXS model mice (Fig. 3H). Overall, these results indicate that the Rac1-PAK1/2-cofilin pathway and the actin polymerization/depolymerization equilibrium are up-regulated in hippocampal area CA1 of FXS model mice.

Actin dynamics are normalized by inhibition of eIF4E-eIF4G interactions in FXS model mice

It has been reported that activation of the Rac1-PAK pathway induced by synaptic activity is defective in the absence of FMRP (*54*). Accumulating evidence indicates that multiple signaling pathways (such as ERK and mTORC1), synaptic plasticity, and structural plasticity are defective in FXS model mice (*25*, *38*, *39*, *41*, *43*, *44*, *46*). Because the aforementioned signaling pathways are downstream of group 1 mGluRs in FXS model mice (*25*, *38*, *39*, *41*, *43*, *44*, *46*), we first asked whether the Rac1-PAK1/2-cofilin signaling pathway that is up-regulated in FXS

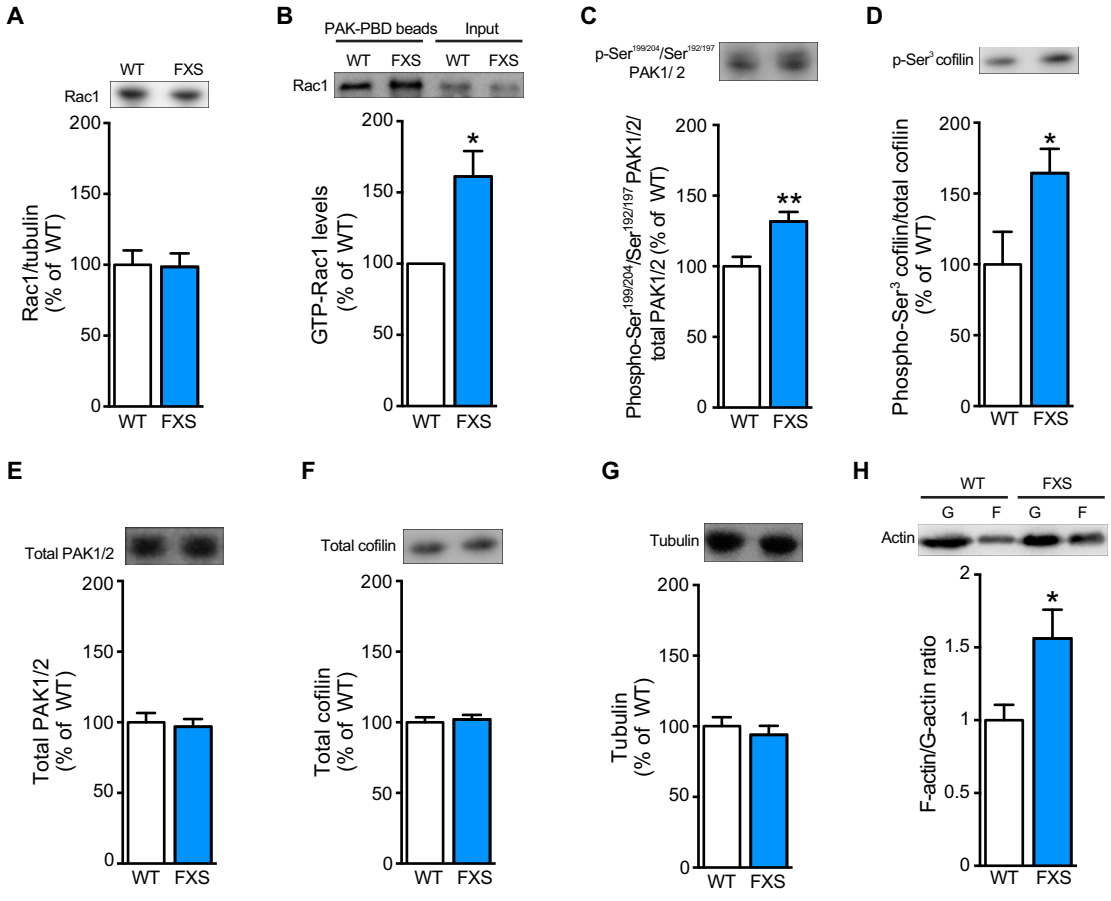

Fig. 3. Rac1-PAK1/2-cofilin signaling and the F-actin/G-actin ratio are increased in FXS model mice. (**A** to **H**) Representative Western blots and quantification assessing the abundance of (A) total Rac1 relative to tubulin (G), (B) Rac1-GTP abundance by PAK-PBD pull-down (t = 3.44), (C) phospho-Ser$^{199/204}$ PAK1 and Ser$^{192/197}$ PAK2 relative to total PAK1/2 (E; t = 3.31), (D) phospho-Ser^{3} cofilin relative to total cofilin (F; t = 2.24), and (H) the F-actin/G-actin ratio (t = 2.51) in the hippocampal CA1 area of FXS model mice and WT littermates. Data are means ± SEM normalized to WT controls. n = 4 to 10 samples per genotype; not significant unless noted; *P < 0.05, **P < 0.01 by Student's t test.

model mice (Fig. 3) is normally activated downstream of group 1 mGluRs. In addition, we blocked eIF4F activity by using 4EGI-1 (*47*, *48*, *75*) to determine whether the signaling pathway regulating actin dynamics is coupled to a signaling pathway regulating protein synthesis.

We performed these experiments with a classic pharmacology cross design by applying DHPG (10 min, 50 μM) and 4EGI-1 (preincubated for at least 40 min, 100 μM) alone or in combination. We found that DHPG significantly increased the phosphorylation of both PAK1/2 and cofilin in wild-type mice and that 4EGI-1 blocked this effect (Fig. 4, A and B). In contrast, the same DHPG treatment failed to significantly alter the phosphorylation of PAK1/2 and cofilin in FXS model mice (Fig. 4, A and B). Moreover, 4EGI-1 reduced the phosphorylation of PAK1/2 and cofilin when administered either alone or in combination with DHPG (Fig. 4, A and B). None of the treatments altered either the amount of tubulin or the total amounts of PAK1/2 and cofilin (Fig. 4, C to E). Overall, these results indicate that the PAK1/2-cofilin pathway is activated by group 1 mGluRs in wild-type mice, mediated at least in part by eIF4E, but that mGluR-induced activation of the pathway is impaired in FXS model mice. Because 4EGI-1 normalized the basal phosphorylation of PAK1/2 and cofilin in FXS model mice, we asked whether it also could restore the increased F-actin/G-actin ratio. We found that 4EGI-1 significantly reduced the F-actin/G-actin ratio in FXS model mice without affecting the ratio in wild-type littermates (Fig. 5, A and B). Thus, inhibition of eIF4E-eIF4G interactions effectively decreases the F-actin/G-actin ratio and the phosphorylation of PAK1/2 and cofilin in FXS model mice.

The results presented thus far indicated that there is enhanced Rac1-PAK1/2-cofilin signaling in FXS model mice, but it was still unclear how 4EGI-1 normalizes this enhancement as well as the synaptic, structural, and behavioral phenotypes (Figs. 1 and 2). It was previously proposed that two pools of CYFIP1 exist, one associated with FMRP/eIF4E (which represses translation of specific mRNAs) and another one where it is bound to Rac1/WRC (which controls actin dynamics) (*67*, *72*, *74*). These complexes are in equilibrium but often compete to bind to free CYFIP1. Thus, we hypothesized that by interfering with eIF4E-eIF4G interactions, 4EGI-1 leads to free eIF4E that may compete with Rac1 to bind CYFIP1 and sequester it from Rac1/WRC. We tested this hypothesis using pull-down assays to determine whether CYFIP1 was preferentially associated with either eIF4E or Rac1 in FXS model mice and whether 4EGI-1 altered these associations. In a first set of experiments performed in hippocampal slices, we found that CYFIP1 was preferentially associated with Rac1 in the FXS model mice (Fig. 5C), which was correlated with decreased binding of CYFIP1 to eIF4E (Fig. 5D). Upon administration of 4EGI-1, we found decreased amounts of CYFIP1 bound to Rac1 (Fig. 5E) and increased amounts of CYFIP1 associated with eIF4E in FXS model mice and their wild-type littermates (Fig. 5F), which is likely due to the competing effects of free eIF4E on CYFIP1. To determine whether this molecular mechanism is also operating in vivo, we performed a similar set of experiments by dissecting the hippocampi of wild-type and FXS model mice 1 hour after intracerebroventricular infusions of 4EGI-1 (100 μM) and used the dissected tissues for pull-down assays. These experiments were designed

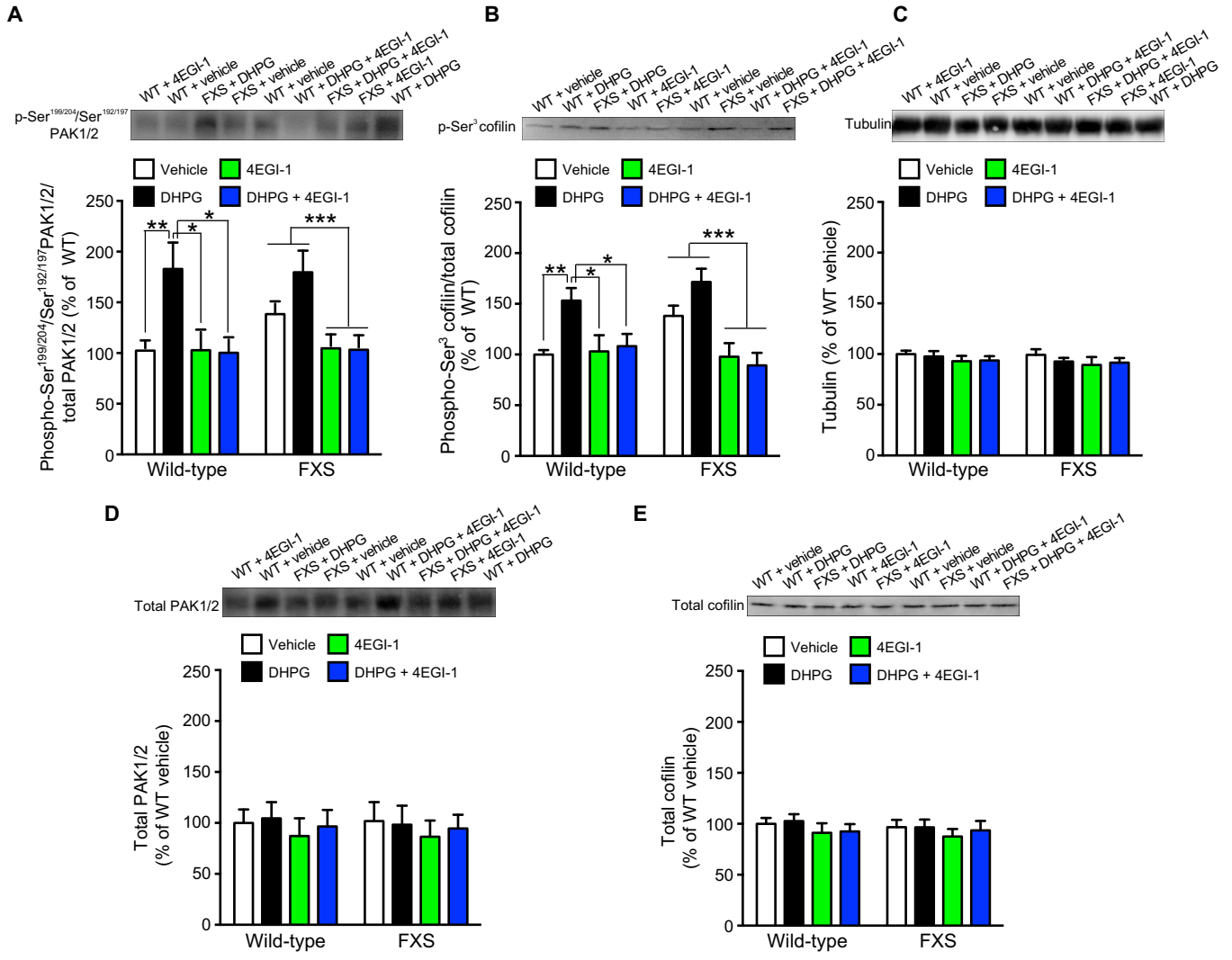

Fig. 4. Rac1-PAK1/2-cofilin signaling pathway is dysregulated in FXS model mice but is normalized by blocking the interaction of eIF4E and eIF4G. (**A** to **E**) Representative Western blots and quantification of (A) phospho-Ser$^{199/204}$/Ser$^{192/197}$ PAK1/2 and (B) phospho-Ser^{3} cofilin, relative to (D) total PAK1/2 or (E) total cofilin, respectively, and of tubulin (C, loading control), in area CA1 of hippocampal slices obtained from WT or FXS mice treated with DHPG (50 μM for 10 min), 4EGI-1 (100 μM; alone or applied 40 min before DHPG), or the combination DHPG and 4EGI-1. $n = 9$ to 22 (WT) or 11 to 17 (FXS) samples per treatment. Data are means ± SEM normalized to WT vehicle-treated controls. Effects of DHPG treatment [$F_{1,47} = 4.76$ (A) and $F_{1,48} = 7.12$ (B)], 4EGI-1 treatment [$F_{1,47} = 5.3$ (A) and $F_{1,48} = 5.06$ (B)], and DHPG + 4EGI-1 treatment [$F_{1,47} = 5.4$ (A) and $F_{1,48} = 6.5$ (B)] in samples from WT mice were significant (analyzed by two-way ANOVA, each $P < 0.05$). ***$P < 0.005$ effect of the 4EGI-1 treatment in FXS model mice [$F_{1,48} = 12.55$ (A) and 18.99 (B)] by two-way ANOVA. (A and B) *$P < 0.05$ and **$P < 0.01$ by Tukey's multiple comparisons test. Data in (C) to (E) are not significantly different.

to determine whether 4EGI-1 was normalizing or simply changing the interactions between CYFIP1, eIF4E, and Rac1. Similar to what we described above (Fig. 5, C and D), we confirmed that at steady state, CYFIP1 is more associated with Rac1 (Fig. 5G) and less associated with eIF4E (Fig. 5H) in FXS model mice. Infusion of 4EGI-1 normalizes these interactions by decreasing the binding of CYFIP1 to Rac1 and increasing the association to eIF4E (Fig. 5, G and H). These results provide a mechanism for how protein synthesis and actin dynamics are regulated to ensure normal synaptic plasticity and behavior in wild-type mice and how these pathways are altered in FXS model mice.

DISCUSSION

Multiple pieces of evidence suggest the involvement of signaling molecules regulating cytoskeleton remodeling and actin dynamics in the structural and synaptic phenotypes displayed by FXS model mice (*67*, *72*, *74*). It has been reported that FMRP and Rac1 are connected in a common signaling pathway and that Rac1 functions are compromised in the absence of FMRP (*67*, *68*). Moreover, either a dominant-negative form of PAK1, which inhibits PAK activity, or pharmacological blockade of PAK1 rescues structural and behavioral alterations displayed by FXS model mice (*69*–*71*). Our discovery of increases in Rac1 activity, phosphorylation of PAK1/2 and cofilin, and F-actin/G-actin ratio is in line with previous studies, suggesting an interaction between Rac1 and FMRP (*67*, *68*, *72*). Our results may help to explain why reduction of PAK phosphorylation/activation is effective in rescuing several phenotypes in FXS model mice (*69*–*71*). It should be noted that in contrast with our findings, a decrease in phosphorylation of cofilin and increased levels of PP2Ac, which is the phosphatase that dephosphorylates cofilin, were reported in murine fibroblast lacking FMRP (*68*).

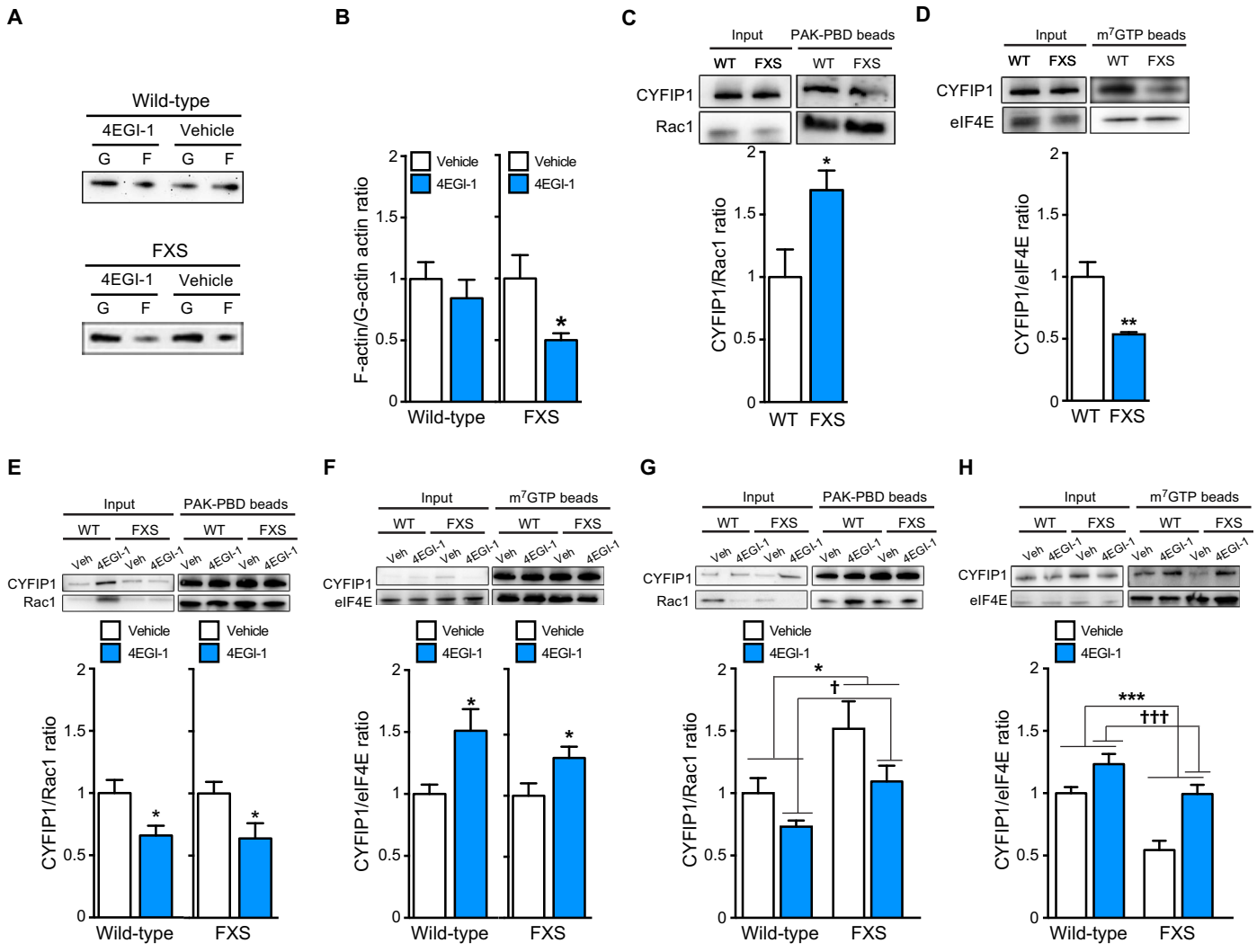

Fig. 5. F-actin/G-actin ratio and preferential binding of CYFIP1 to Rac1 in FXS model mice are normalized by administration of 4EGI-1. (**A** and **B**) Representative Western blot (A) and quantification (B) of F-actin relative to G-actin abundance in WT or FXS hippocampal slices treated with 4EGI-1 or vehicle. n = 9 to 10 (WT) or 7 (FXS) samples per genotype. t = 2.54 (FXS). *P < 0.05 by Student's t test. (**C** and **D**) Representative Western blots and quantification of pull-down assays with PAK-PBD beads (C) or m^{7}GTP beads (D) performed on lysates of hippocampal slices from WT (WT) or FXS mice. n = 4 (C) or 3 (D) samples per genotype. t = 2.56 (C) and 3.86 (D). *P < 0.05 by Student's t test. (**E** and **F**) Representative Western blots and quantification of pull-down assays performed as described for (C) and (D) in hippocampal slices treated with 4EGI-1 (100 μM or equivalent volume of vehicle). Data are means ± SEM normalized to their respective vehicle controls. n = 4 to 5 (WT) or 6 to 7 (FXS) samples per genotype. (E) t = 2.60 (WT) and 2.40 (FXS); (F) t = 2.46 (WT) and 2.23 (FXS). *P < 0.05, **P < 0.01, Student's t test. (**G** and **H**) Representative Western blots and quantification of pull-down assays performed in hippocampi dissected 1 hour after intracerebroventricular infusions with 4EGI-1 (100 μM) or equivalent volume of vehicle. Data are means ± SEM normalized to WT vehicle controls. n = 4 mice per genotype per treatment. *P < 0.05, ***P < 0.005, †P < 0.05, †††P < 0.005, effects of treatment [$F_{1,11}$ = 5.03 (G) and $F_{1,12}$ = 23.12 (H)] and genotype [$F_{1,11}$ = 8.16 (G) and $F_{1,12}$ = 23.95 (H)], analyzed by two-way ANOVA.

The difference between these findings is most likely due to the difference in the models (cell culture versus brain slices) and/or cell types (fibroblasts versus neurons) used in the two studies. In the future, it will be interesting to address whether Rac1-PAK1/2-cofilin signaling is elevated in the brains of FXS patients.

We found that activation of group 1 mGluR receptors triggers the activation of the PAK1/2-cofilin signaling pathway that regulates actin dynamics in area CA1 of the hippocampus in wild-type mice. In contrast, when we examined the effect of mGluR activation on the activity of the PAK1/2-cofilin pathway in FXS model mice, we did not observe further increases, suggesting that this signaling pathway is already at plateau. This result is consistent with several previous reports demonstrating the decoupling of mGluRs from downstream signaling pathways in FXS model mice. For instance, baseline phosphorylation of p70 ribosomal protein S6 kinase 1 (S6K1) and eIF4E-eIF4G interactions, which are downstream effectors of the mTORC1 and ERK pathways and link mGluRs to the protein synthesis machinery, are already elevated in FXS model mice and are not stimulated further by activation of group 1 mGluRs (*38*, *39*). Moreover, stimulation of group 1 mGluRs leads to enhanced hippocampal LTD in FXS model mice but no longer requires activation of ERK and mTORC1, or de novo protein synthesis (*27*, *82*, *83*, *88*). Consistent with our findings, it was demonstrated that Rac1-PAK1 activation induced by synaptic activity is defective in the hippocampus of FXS model mice (*54*). In this context, our results indicate

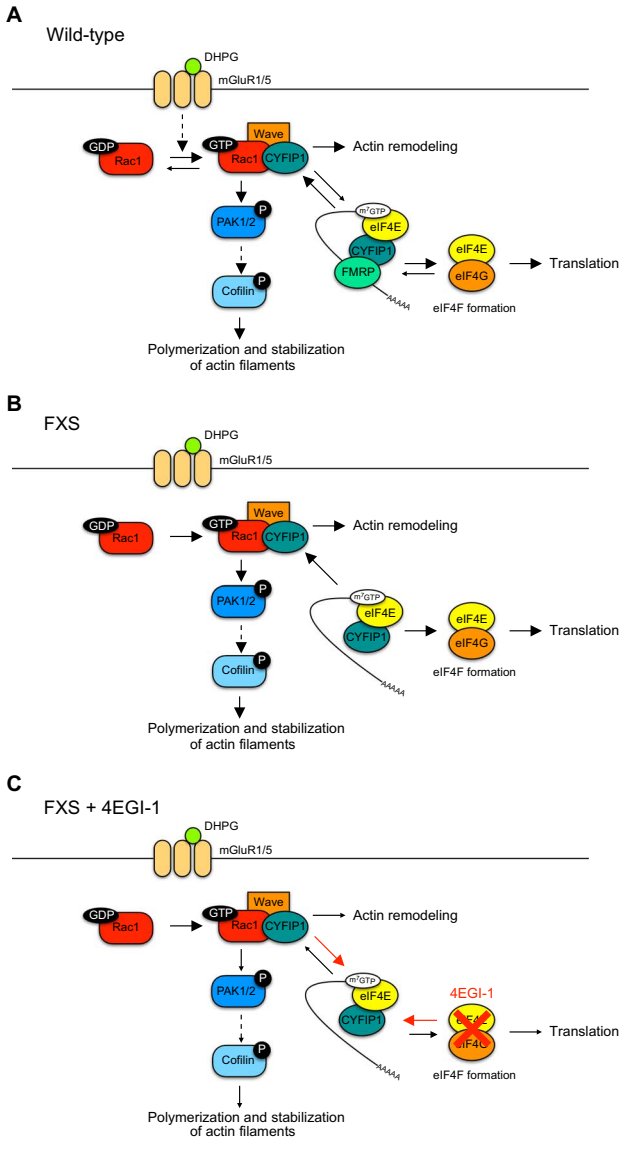

Fig. 6. Proposed model for the coordinated interaction of protein synthesis and dendritic spine dynamics induced by activation of mGluR1/5. (**A**) In area CA1 of the hippocampus in WT mice, CYFIP1 is present in two macromolecular complexes: CYFIP1-FMRP-eIF4E, which represses translation, and CYFIP1-WRC-Rac1-GTP, which regulates actin remodeling. Activation of mGluR1/5 changes the balance between these two complexes by increasing the activation of Rac1 and downstream signaling molecules and inducing protein synthesis via the relocation of CYFIP1 to the WRC-Rac1-GTP complex. The concomitant change in these signaling pathways ensures normal physiological synaptic plasticity and higher brain function. (**B**) In FXS model mice, the signaling molecules regulating protein synthesis and actin dynamics are no longer regulated by activation of mGluR1/5. Moreover, the absence of FMRP leads to exaggerated protein synthesis, perhaps via enhanced association of eIF4E to eIF4G. The lack of FMRP also results in an alteration in actin dynamics via enhanced Rac1-GTP abundance and increased association of CYFIP1 to WRC-Rac1-GTP. The disruption of these two signaling modules results in aberrant synaptic plasticity, spine morphology, and brain function that are characteristic of FXS. (**C**) 4EGI-1 restores the balance between protein synthesis and actin dynamics by creating free eIF4E that competes with Rac1-GTP to bind CYFIP1. This normalizes the aberrant synaptic plasticity, spine morphology, and cognitive function exhibited in FXS model mice. Dashed arrows indicate an indirect phosphorylation mechanism. Thick and thin arrows indicate enhanced and reduced interactions, respectively. Red arrows indicate the effect of 4EGI-1.

that the Rac1-PAK1/2-cofilin pathway is altered and uncoupled to group1 mGluR activity in FXS mice, as was previously shown for mTORC1 and ERK signaling, as well as de novo protein synthesis.

Notably, we found that blocking eIF4E-eIF4G interactions with 4EGI-1, which is increased in FXS model mice (*38*, *40*), normalizes Rac1-PAK1/2-cofilin signaling (Fig. 4), synaptic plasticity (Fig. 2), context discrimination, and spine density (Fig. 1) phenotypes in FXS model mice. 4EGI-1 is an inhibitor of cap-dependent protein synthesis, which, by blocking the association of eIF4E with eIF4G, prevents the formation of the eIF4F initiation complex (*47*, *48*, *75*, *76*). The effects of 4EGI-1 on Rac1-PAK1/2-cofilin signaling are observed both in the baseline condition for FXS model mice and after DHPG stimulation in both wild-type and FXS model mice, suggesting that interfering with eIF4E-eIF4G interactions is beneficial in the absence of FMRP. From a molecular standpoint, it is possible that these multiple phenotypic rescues mediated by 4EGI-1 in FXS model mice have more than one explanation.

Many of the phenotypes displayed by FXS model mice are rescued by interfering with components of the mTORC1 and ERK pathways, both of which regulate protein synthesis downstream of group 1 mGluRs (*39*, *41*, *43*, *44*). For example, either genetically or pharmacologically inhibiting the mTORC1 substrate S6K1 (*41*, *43*) or the ERK-dependent phosphorylation of eIF4E (*39*) can rescue multiple phenotypes in FXS model mice. Notably, eIF4E-eIF4G interactions are enhanced in FXS model mice (*38*, *40*) and both mTORC1 and ERK activation increase the levels of eIF4E-eIF4G interactions to initiate protein synthesis (*89*–*91*). At the same time, normalization of multiple phenotypes displayed by FXS mice can also be achieved by either genetically or pharmacologically inhibiting the activity of PAK1 (*69*, *70*).

Our data are consistent with a model describing CYFIP1 as a molecule regulating protein synthesis and actin dynamics by shuttling between the FMRP/eIF4E and Rac1/WRC complexes (*9*, *67*, *72*). Our results indicate that, at baseline, CYFIP1 is preferentially associated with Rac1, possibly in the WRC complex, rather than eIF4E, in FXS model mice (Fig. 6B). Administration of 4EGI-1 inhibits the association of eIF4E to eIF4G and creates free eIF4E that competes with Rac1 to bind CYFIP1, thus restoring the balance between these signaling pathways (Fig. 6C). Although the precise molecular details linking the interaction of Rac1 to CYFIP1 (with the effect on PAK1/2-cofilin signaling by 4EGI-1) are unclear, it is possible that Rac1 becomes less effective in activating the downstream PAK1/2-cofilin in the absence of CYFIP1. In the future, it will be interesting to investigate the molecular details of these interactions.

In summary, our results support a model that links dysregulated protein synthesis with altered actin dynamics in FXS, and underscore the importance of a balanced regulation of these two pathways for a normal brain function (Fig. 6). Moreover, our results suggest an alternative way to counteract the abnormal phenotypes displayed by FXS model mice, which can be pursued by using drugs that normalize both molecular pathways.

MATERIALS AND METHODS

Animals

All procedures involving animals were performed in accordance with protocols approved by the New York University Animal Welfare Committee and followed the National Institutes of Health (NIH) *Guide for the Care and Use of Laboratory Animals*. All mice were housed in the New York University animal facility and were compliant

with the NIH *Guide for the Care and Use of Laboratory Animals*. Male *Fmr1* knockout mice and wild-type littermates were used in all experiments. *Fmr1* knockout mice and their wild-type littermates were bred and maintained on a C57/BL6 (Jackson Labs) background as previously described (*82*, *92*). Mice were housed with their littermates in groups of two to three animals per cage and kept on a 12-hour regular light/dark cycle, with food and water provided ad libitum. All the data presented in this study were collected and analyzed with the experimenters blind to genotype and/or treatment.

Biochemistry

Biochemistry experiments were performed on transverse hippocampal slices (400 μm) from 3- to 6-week-old male mice in Figs. 3, 4, and 5 (A to F) and from 3-month-old male mice in Fig. 5 (G and H). Pull-down assays, F-actin/G-actin measurements, and Western blots were performed routinely as described previously (*9*, *72*, *92*). Briefly, Western blots were performed from microdissected CA1 hippocampal lysates (presented in Figs. 3, A to G, and 4; four to six slices per sample), whereas in pull-down assays and the F-actin/G-actin experiments, we used whole hippocampal slices (presented in Figs. 3H and 5, A to F; four to six slices per samples).

Hippocampal slices were prepared and incubated at 37°C in artificial cerebrospinal fluid (aCSF) for 2 hours as described previously (*93*–*95*). At the end of this incubation period, the following drugs, or equivalent volumes of vehicle, were bath-applied: DHPG (50 μM; 10 min) and 4EGI-1 (100 μM; 40 min before incubation plus 10 min with either vehicle or DHPG). All the slices were removed from the aCSF and rapidly flash-frozen on dry ice. The tissues were sonicated in 1% SDS and then boiled for 10 min. Aliquots of the homogenate were used to determine the protein content with the Pierce BCA Protein Assay Kit (Thermo Fisher Scientific). An equal amount of protein (30 μg) was loaded onto 10% polyacrylamide gels, and proteins were separated by SDS–polyacrylamide gel electrophoresis followed by overnight transfer to polyvinylidene difluoride membranes (GE Healthcare).

The tissues used for F-actin/G-actin experiments were sonicated in a cold lysis buffer containing 10 mM K_2HPO_4, 100 mM NaF, 50 mM KCl, 2 mM $MgCl_2$, 1 mM EGTA, 0.2 mM dithiothreitol (DTT), 0.5% Triton X-100, 1 mM sucrose (pH 7.0) and centrifuged at 15,000*g* for 30 min. The supernatant was collected to measure the soluble form of actin (G-actin). The pellet containing the insoluble form of actin (F-actin) was resuspended in lysis buffer plus an equal volume of a second buffer containing 1.5 mM guanidine hydrochloride, 1 mM sodium acetate, 1 mM $CaCl_2$, 1 mM adenosine triphosphate, 20 mM tris-HCl (pH 7.5) and incubated on ice for 1 hour with gentle mixing every 15 min. The samples were centrifuged at 15,000*g* for 30 min, and the supernatant containing F-actin was collected. Samples from the supernatant (G-actin) and pellet (F-actin) were loaded in equal amount and analyzed on Western blots.

Pull-down assays were performed in young (3- to 6-week-old, hippocampal slices) and adult (3-month-old) mice. In the adult mice, hippocampi were dissected 1 hour after intracerebroventricular infusions with 4EGI-1 (100 μM; or an equivalent volume of vehicle) and flash-frozen on dry ice. All the tissues were sonicated in cold lysis buffer containing 150 mM NaCl, 10 mM $MgCl_2$, 30 mM tris buffer (pH 8.0), 1 mM DTT, 1.5% Triton X-100, protease and ribonuclease inhibitors. The lysate (500 μg) was incubated with either 20 to 30 μl of PAK-PBD (Cytoskeleton Inc) or m^7GTP beads (Jena Bioscience) for 2 hours at 4°C. The beads were centrifuged for 1 min at 6000 rpm, and the supernatant was collected. The beads were then washed three times in wash buffer [100 mM KCl, 50 mM tris buffer (pH 7.4), 5 mM $MgCl_2$, 0.5% Triton X-100]. Finally, the beads were eluted with 50 to 100 μl of Laemmli buffer and analyzed on Western blots.

The following antibodies were used in the Western blot experiments: phospho-PAK1 ($Ser^{199/204}$)/PAK2 ($Ser^{192/197}$), PAK1/2, phospho-cofilin (Ser^3), cofilin (1:500; Cell Signaling Technology), and tubulin (1:5000; Cell Signaling Technology), which was used to determine the total amounts of the proteins. Additional antibodies included Rac1 (1:2000; BD Transduction Laboratories), CYFIP1 (1:1000; Millipore), eIF4E (1:1000; Bethyl Laboratories), and actin (1:10,000; Millipore).

Slice electrophysiology

All electrophysiology experiments were performed on transverse hippocampal slices (400 um) from 3- to 6-week-old male mice. Slice preparation, aCSF composition, and all mGluR-LTD experiments were performed as described previously (*93*–*95*). Briefly, DHPG was bath-applied for 10 min at 50 μM (final concentration), 4EGI-1 at least 40 min before incubation at 100 μM, and anisomycin during baseline at 20 μM. 4EGI-1 and anisomycin were maintained in the bath for the duration of the recordings. Similar doses were used previously in experiments of synaptic plasticity in brain slices (*33*, *38*, *48*, *96*). DHPG and anisomycin were purchased at Tocris and diluted according to the manufacturing instructions. 4EGI-1 was purchased at Calbiochem/Millipore and diluted as described in (*47*, *48*, *75*, *81*). Vehicle-treated slices received equivalent volumes of the diluents.

Surgery

Adult (3-month-old) male mice received surgery, where cannulae were unilaterally implanted in the right lateral ventricle as described previously (*48*, *81*). Briefly, mice were anesthetized with ketamine (100 mg/kg) and xylazine (10 mg/kg) and mounted on a stereotaxic apparatus. Cannulae (26-gauge; Plastics One) were implanted at the following coordinates: 20.22 mm anteroposterior, 11 mm mediolateral, and 22.4 mm dorsoventral (*48*, *81*). Mice were given at least 1 week after surgery to recover.

Neuroanatomy

4EGI-1 was prepared and infused as previously described (*47*, *48*, *75*, *81*). Briefly, infusions of 4EGI-1 (1 μl at 100 μM; or vehicle) were administered over 1 min (0.5 μl/min) (Harvard Apparatus), and injectors remain in the guide cannulae for 2 min after infusion (*81*). Mice were sacrificed 24 hours after the infusions, and the brains were rapidly dissected and prepared for the staining procedure using the Rapid Golgi Kit (FD NeuroTechnologies) as previously described (*41*, *70*). Briefly, brain sections (200 μm) were imaged on an Olympus BX51 light microscope using Neurolucida software (MBF Bioscience) with 100×/numerical aperture 1.4 immersion oil. Apical dendrites of pyramidal neurons from hippocampal area CA1 located in the stratum radiatum were traced from each animal, and spine densities were measured by counting the number of spines along a 60-μm dendritic segment, at intervals of 10 μm, from traces exported and analyzed using Neurolucida Explorer. Spines were characterized as either immature (filopodia and long thin) or mature (stubby, mushroom, and branched) on the basis of the shape of each spine as previously described (*41*, *43*).

Context discrimination

Mice were trained in two contexts for two consecutive days: a context in which they received a shock (S+) and a context in which they did not receive a shock (S−). The S+ context consisted of a plexiglass

chamber, with metal grid flooring in which a 0.5-mA shock was delivered after 3 min. The S– context consisted of a clear plexiglass chamber, illuminated by a red house light, a white, opaque plexiglass floor that was covered with vanilla-scented bedding; mice spent 3 min in this context, and no shock was delivered. The intertrial interval between context exposures was 1.5 hours. On day 2 of context discrimination, FXS model mice and their wild-type littermates received an infusion of either 4EGI-1 or vehicle 1 hour before exposure to the S– context. 4EGI-1 (1 μl at 100 μM; or equivalent volume of vehicle) was infused over 1 min (0.5 μl/min) (Harvard Apparatus), and injectors remained in the guide cannulae for 2 min after infusion as previously described in (*81*). Mice were placed in the S– context (*79*) 1 hour after the infusions. All groups were exposed to the S+ context 1.5 hours after exposure to the S– context. Freezing behavior to S+ and S– contexts is represented as discrimination index calculated by the percentage of time spent freezing in the S– context divided for the percentage of time spent freezing in the S+ context.

Statistical analysis

Biochemical data (comparing FXS model mice and wild-type littermates) and electrophysiology data (comparing vehicle and 4EGI-1) were analyzed with either Student's *t* tests or one-sample *t* tests. Biochemical data with pharmacological treatments and context discrimination data were analyzed using two-way ANOVA, in which DHPG and 4EGI-1 or time and treatment, respectively, were the independent variables, followed by Tukey's post hoc test. Cumulative spine density data were analyzed using two-way ANOVA followed by Dunnett's post hoc test. Outliers were detected with the Grubbs' test and excluded from the analysis.

REFERENCES AND NOTES

1. W. T. O'Donnell, S. T. Warren, A decade of molecular studies of fragile X syndrome. *Annu. Rev. Neurosci.* **25**, 315–338 (2002).
2. G. J. Bassell, S. T. Warren, Fragile X syndrome: Loss of local mRNA regulation alters synaptic development and function. *Neuron* **60**, 201–214 (2008).
3. J. C. Darnell, E. Klann, The translation of translational control by FMRP: Therapeutic targets for FXS. *Nat. Neurosci.* **16**, 1530–1536 (2013).
4. C. Bagni, W. T. Greenough, From mRNP trafficking to spine dysmorphogenesis: The roots of fragile X syndrome. *Nat. Rev. Neurosci.* **6**, 376–387 (2005).
5. J. B. Dictenberg, S. A. Swanger, L. N. Antar, R. H. Singer, G. J. Bassell, A direct role for FMRP in activity-dependent dendritic mRNA transport links filopodial-spine morphogenesis to fragile X syndrome. *Dev. Cell* **14**, 926–939 (2008).
6. J. C. Darnell, S. J. Van Driesche, C. Zhang, K. Y. S. Hung, A. Mele, C. E. Fraser, E. F. Stone, C. Chen, J. J. Fak, S. W. Chi, D. D. Licatalosi, J. D. Richter, R. B. Darnell, FMRP stalls ribosomal translocation on mRNAs linked to synaptic function and autism. *Cell* **146**, 247–261 (2011).
7. M. Qin, J. Kang, T. V. Burlin, C. Jiang, C. B. Smith, Postadolescent changes in regional cerebral protein synthesis: An in vivo study in the *Fmr1* null mouse. *J. Neurosci.* **25**, 5087–5095 (2005).
8. J. Marcotrigiano, A.-C. Gingras, N. Sonenberg, S. K. Burley, Cap-dependent translation initiation in eukaryotes is regulated by a molecular mimic of eIF4G. *Mol. Cell* **3**, 707–716 (1999).
9. I. Napoli, V. Mercaldo, P. P. Boyl, B. Eleuteri, F. Zalfa, S. De Rubeis, D. Di Marino, E. Mohr, M. Massimi, M. Falconi, W. Witke, M. Costa-Mattioli, N. Sonenberg, T. Achsel, C. Bagni, The fragile X syndrome protein represses activity-dependent translation through CYFIP1, a new 4E-BP. *Cell* **134**, 1042–1054 (2008).
10. J. D. Richter, N. Sonenberg, Regulation of cap-dependent translation by eIF4E inhibitory proteins. *Nature* **433**, 477–480 (2005).
11. J. L. Banko, M. Merhav, E. Stern, N. Sonenberg, K. Rosenblum, E. Klann, Behavioral alterations in mice lacking the translation repressor 4E-BP2. *Neurobiol. Learn. Mem.* **87**, 248–256 (2007).
12. J. L. Banko, L. Hou, F. Poulin, N. Sonenberg, E. Klann, Regulation of eukaryotic initiation factor 4E by converging signaling pathways during metabotropic glutamate receptor-dependent long-term depression. *J. Neurosci.* **26**, 2167–2173 (2006).
13. J. L. Banko, F. Poulin, L. Hou, C. T. DeMaria, N. Sonenberg, E. Klann, The translation repressor 4E-BP2 is critical for eIF4F complex formation, synaptic plasticity, and memory in the hippocampus. *J. Neurosci.* **25**, 9581–9590 (2005).
14. A.-C. Gingras, S. G. Kennedy, M. A. O'Leary, N. Sonenberg, N. Hay, 4E-BP1, a repressor of mRNA translation, is phosphorylated and inactivated by the Akt(PKB) signaling pathway. *Genes Dev.* **12**, 502–513 (1998).
15. M.-Y. Jung, L. Lorenz, J. D. Richter, Translational control by neuroguidin, a eukaryotic initiation factor 4E and CPEB binding protein. *Mol. Cell. Biol.* **26**, 4277–4287 (2006).
16. N. Hay, N. Sonenberg, Upstream and downstream of mTOR. *Genes Dev.* **18**, 1926–1945 (2004).
17. C. M. Fletcher, A. M. McGuire, A.-C. Gingras, H. Li, H. Matsuo, N. Sonenberg, G. Wagner, 4E binding proteins inhibit the translation factor eIF4E without folded structure. *Biochemistry* **37**, 9–15 (1998).
18. S. J. Tang, G. Reis, H. Kang, A.-C. Gingras, N. Sonenberg, E. M. Schuman, A rapamycin-sensitive signaling pathway contributes to long-term synaptic plasticity in the hippocampus. *Proc. Natl. Acad. Sci. U.S.A.* **99**, 467–472 (2002).
19. A. J. Waskiewicz, J. C. Johnson, B. Penn, M. Mahalingam, S. R. Kimball, J. A. Cooper, Phosphorylation of the cap-binding protein eukaryotic translation initiation factor 4E by protein kinase Mnk1 in vivo. *Mol. Cell. Biol.* **19**, 1871–1880 (1999).
20. R. J. Kelleher III, A. Govindarajan, H.-Y. Jung, H. Kang, S. Tonegawa, Translational control by MAPK signaling in long-term synaptic plasticity and memory. *Cell* **116**, 467–479 (2004).
21. A. J. Waskiewicz, A. Flynn, C. G. Proud, J. A. Cooper, Mitogen-activated protein kinases activate the serine/threonine kinases Mnk1 and Mnk2. *EMBO J.* **16**, 1909–1920 (1997).
22. I. J. Weiler, S. A. Irwin, A. Y. Klintsova, C. M. Spencer, A. D. Brazelton, K. Miyashiro, T. A. Comery, B. Patel, J. Eberwine, W. T. Greenough, Fragile X mental retardation protein is translated near synapses in response to neurotransmitter activation. *Proc. Natl. Acad. Sci. U.S.A.* **94**, 5395–5400 (1997).
23. M. S. Sidorov, B. D. Auerbach, M. F. Bear, Fragile X mental retardation protein and synaptic plasticity. *Mol. Brain* **6**, 15 (2013).
24. M. W. Waung, K. M. Huber, Protein translation in synaptic plasticity: mGluR-LTD, fragile X. *Curr. Opin. Neurobiol.* **19**, 319–326 (2009).
25. E. Klann, J. D. Sweatt, Altered protein synthesis is a trigger for long-term memory formation. *Neurobiol. Learn. Mem.* **89**, 247–259 (2008).
26. J. D. Richter, G. J. Bassell, E. Klann, Dysregulation and restoration of translational homeostasis in fragile X syndrome. *Nat. Rev. Neurosci.* **16**, 595–605 (2015).
27. K. M. Huber, S. M. Gallagher, S. T. Warren, M. F. Bear, Altered synaptic plasticity in a mouse model of fragile X mental retardation. *Proc. Natl. Acad. Sci. U.S.A.* **99**, 7746–7750 (2002).
28. J. Li, M. R. Pelletier, J.-L. Perez Velazquez, P. L. Carlen, Reduced cortical synaptic plasticity and GluR1 expression associated with fragile X mental retardation protein deficiency. *Mol. Cell. Neurosci.* **19**, 138–151 (2002).
29. M.-G. Zhao, H. Toyoda, S. W. Ko, H.-K. Ding, L.-J. Wu, M. Zhuo, Deficits in trace fear memory and long-term potentiation in a mouse model for fragile X syndrome. *J. Neurosci.* **25**, 7385–7392 (2005).
30. R. C. Malenka, M. F. Bear, LTP and LTD: An embarrassment of riches. *Neuron* **44**, 5–21 (2004).
31. C. Lüscher, K. M. Huber, Group 1 mGluR-dependent synaptic long-term depression: Mechanisms and implications for circuitry and disease. *Neuron* **65**, 445–459 (2010).
32. I. J. Weiler, W. T. Greenough, Metabotropic glutamate receptors trigger postsynaptic protein synthesis. *Proc. Natl. Acad. Sci. U.S.A.* **90**, 7168–7171 (1993).
33. K. M. Huber, M. S. Kayser, M. F. Bear, Role for rapid dendritic protein synthesis in hippocampal mGluR-dependent long-term depression. *Science* **288**, 1254–1256 (2000).
34. C. Job, J. Eberwine, Identification of sites for exponential translation in living dendrites. *Proc. Natl. Acad. Sci. U.S.A.* **98**, 13037–13042 (2001).
35. M. F. Bear, K. M. Huber, S. T. Warren, The mGluR theory of fragile X mental retardation. *Trends Neurosci.* **27**, 370–377 (2004).
36. G. Dölen, E. Osterweil, B. S. S. Rao, G. B. Smith, B. D. Auerbach, S. Chattarji, M. F. Bear, Correction of fragile X syndrome in mice. *Neuron* **56**, 955–962 (2007).
37. E. K. Osterweil, D. D. Krueger, K. Reinhold, M. F. Bear, Hypersensitivity to mGluR5 and ERK1/2 leads to excessive protein synthesis in the hippocampus of a mouse model of fragile X syndrome. *J. Neurosci.* **30**, 15616–15627 (2010).
38. A. Sharma, C. A. Hoeffer, Y. Takayasu, T. Miyawaki, S. M. McBride, E. Klann, R. S. Zukin, Dysregulation of mTOR signaling in fragile X syndrome. *J. Neurosci.* **30**, 694–702 (2010).
39. C. G. Gkogkas, A. Khoutorsky, R. Cao, S. M. Jafarnejad, M. Prager-Khoutorsky, N. Giannakas, A. Kaminari, A. Fragkouli, K. Nader, T. J. Price, B. W. Konicek, J. R. Graff, A. K. Tzinia, J.-C. Lacaille, N. Sonenberg, Pharmacogenetic inhibition of eIF4E-dependent *Mmp9* mRNA translation reverses fragile X syndrome-like phenotypes. *Cell Rep.* **9**, 1742–1755 (2014).
40. J. A. Ronesi, K. A. Collins, S. A. Hays, N.-P. Tsai, W. Guo, S. G. Birnbaum, J.-H. Hu, P. F. Worley, J. R. Gibson, K. M. Huber, Disrupted Homer scaffolds mediate abnormal mGluR5 function in a mouse model of fragile X syndrome. *Nat. Neurosci.* **15**, 431–440 (2012).

41. A. Bhattacharya, H. Kaphzan, A. C. Alvarez-Dieppa, J. P. Murphy, P. Pierre, E. Klann, Genetic removal of p70 S6 kinase 1 corrects molecular, synaptic, and behavioral phenotypes in fragile X syndrome mice. *Neuron* **76**, 325–337 (2012).
42. A. Bhattacharya, E. Klann, Fragile X syndrome therapeutics S(C)TEP through the developmental window. *Neuron* **74**, 1–3 (2012).
43. A. Bhattacharya, M. Mamcarz, C. Mullins, A. Choudhury, R. G. Boyle, D. G. Smith, D. W. Walker, E. Klann, Targeting translation control with p70 S6 kinase 1 inhibitors to reverse phenotypes in fragile X syndrome mice. *Neuropsychopharmacology* **41**, 1991–2000 (2016).
44. E. K. Osterweil, S.-C. Chuang, A. A. Chubykin, M. Sidorov, R. Bianchi, R. K. S. Wong, M. F. Bear, Lovastatin corrects excess protein synthesis and prevents epileptogenesis in a mouse model of fragile X syndrome. *Neuron* **77**, 243–250 (2013).
45. C. A. Hoeffer, E. Klann, mTOR signaling: At the crossroads of plasticity, memory and disease. *Trends Neurosci.* **33**, 67–75 (2010).
46. R. J. Kelleher III, M. F. Bear, The autistic neuron: Troubled translation? *Cell* **135**, 401–406 (2008).
47. C. G. Gkogkas, A. Khoutorsky, I. Ran, E. Rampakakis, T. Nevarko, D. B. Weatherill, C. Vasuta, S. Yee, M. Truitt, P. Dallaire, F. Major, P. Lasko, D. Ruggero, K. Nader, J.-C. Lacaille, N. Sonenberg, Autism-related deficits via dysregulated eIF4E-dependent translational control. *Nature* **493**, 371–377 (2013).
48. E. Santini, T. N. Huynh, A. F. MacAskill, A. G. Carter, P. Pierre, D. Ruggero, H. Kaphzan, E. Klann, Exaggerated translation causes synaptic and behavioural aberrations associated with autism. *Nature* **493**, 411–415 (2013).
49. M. Chahrour, B. J. O'Roak, E. Santini, R. C. Samaco, R. J. Kleiman, M. C. Manzini, Current perspectives in autism spectrum disorder: From genes to therapy. *J. Neurosci.* **36**, 11402–11410 (2016).
50. E. Santini, E. Klann, Reciprocal signaling between translational control pathways and synaptic proteins in autism spectrum disorders. *Sci. Signal.* **7**, re10 (2014).
51. L. A. Cingolani, Y. Goda, Actin in action: The interplay between the actin cytoskeleton and synaptic efficacy. *Nat. Rev. Neurosci.* **9**, 344–356 (2008).
52. G. Lynch, C. S. Rex, C. M. Gall, LTP consolidation: Substrates, explanatory power, and functional significance. *Neuropharmacology* **52**, 12–23 (2007).
53. L. Y. Chen, C. S. Rex, M. S. Casale, C. M. Gall, G. Lynch, Changes in synaptic morphology accompany actin signaling during LTP. *J. Neurosci.* **27**, 5363–5372 (2007).
54. L. Y. Chen, C. S. Rex, A. H. Babayan, E. A. Kramár, G. Lynch, C. M. Gall, J. C. Lauterborn, Physiological activation of synaptic Rac>PAK (p-21 activated kinase) signaling is defective in a mouse model of fragile X syndrome. *J. Neurosci.* **30**, 10977–10984 (2010).
55. R. D. Rudelli, W. T. Brown, K. Wisniewski, E. C. Jenkins, M. Laure-Kamionowska, F. Connell, H. M. Wisniewski, Adult fragile X syndrome. Clinico-neuropathologic findings. *Acta Neuropathol.* **67**, 289–295 (1985).
56. S. A. Irwin, R. Galvez, W. T. Greenough, Dendritic spine structural anomalies in fragile-X mental retardation syndrome. *Cereb. Cortex* **10**, 1038–1044 (2000).
57. W. Huang, P. J. Zhu, S. Zhang, H. Zhou, L. Stoica, M. Galiano, K. Krnjević, G. Roman, M. Costa-Mattioli, mTORC2 controls actin polymerization required for consolidation of long-term memory. *Nat. Neurosci.* **16**, 441–448 (2013).
58. L. Luo, T. K. Hensch, L. Ackerman, S. Barbel, L. Y. Jan, Y. N. Jan, Differential effects of the Rac GTPase on Purkinje cell axons and dendritic trunks and spines. *Nature* **379**, 837–840 (1996).
59. A. Y. Nakayama, M. B. Harms, L. Luo, Small GTPases Rac and Rho in the maintenance of dendritic spines and branches in hippocampal pyramidal neurons. *J. Neurosci.* **20**, 5329–5338 (2000).
60. A. Tashiro, A. Minden, R. Yuste, Regulation of dendritic spine morphology by the Rho family of small GTPases: Antagonistic roles of Rac and Rho. *Cereb. Cortex* **10**, 927–938 (2000).
61. A. Harwood, V. M. M. Braga, Cdc42 & GSK-3: Signals at the crossroads. *Nat. Cell Biol.* **5**, 275–277 (2003).
62. J. Chelly, J.-L. Mandel, Monogenic causes of X-linked mental retardation. *Nat. Rev. Genet.* **2**, 669–680 (2001).
63. D. C. Edwards, L. C. Sanders, G. M. Bokoch, G. N. Gill, Activation of LIM-kinase by Pak1 couples Rac/Cdc42 GTPase signalling to actin cytoskeletal dynamics. *Nat. Cell Biol.* **1**, 253–259 (1999).
64. S. Arber, F. A. Barbayannis, H. Hanser, C. Schneider, C. A. Stanyon, O. Bernard, P. Caroni, Regulation of actin dynamics through phosphorylation of cofilin by LIM-kinase. *Nature* **393**, 805–809 (1998).
65. N. Yang, O. Higuchi, K. Ohashi, K. Nagata, A. Wada, K. Kangawa, E. Nishida, K. Mizuno, Cofilin phosphorylation by LIM-kinase 1 and its role in Rac-mediated actin reorganization. *Nature* **393**, 809–812 (1998).
66. K. Mizuno, Signaling mechanisms and functional roles of cofilin phosphorylation and dephosphorylation. *Cell. Signal.* **25**, 457–469 (2013).
67. A. Schenck, B. Bardoni, C. Langmann, N. Harden, J.-L. Mandel, A. Giangrande, CYFIP/Sra-1 controls neuronal connectivity in *Drosophila* and links the Rac1 GTPase pathway to the fragile X protein. *Neuron* **38**, 887–898 (2003).
68. M. Castets, C. Schaeffer, E. Bechara, A. Schenck, E. W. Khandjian, S. Luche, H. Moine, T. Rabilloud, J.-L. Mandel, B. Bardoni, FMRP interferes with the Rac1 pathway and controls actin cytoskeleton dynamics in murine fibroblasts. *Hum. Mol. Genet.* **14**, 835–844 (2005).
69. M. L. Hayashi, S.-Y. Choi, B. S. S. Rao, H.-Y. Jung, H.-K. Lee, D. Zhang, S. Chattarji, A. Kirkwood, S. Tonegawa, Altered cortical synaptic morphology and impaired memory consolidation in forebrain-specific dominant-negative PAK transgenic mice. *Neuron* **42**, 773–787 (2004).
70. M. L. Hayashi, B. S. S. Rao, J.-S. Seo, H.-S. Choi, B. M. Dolan, S.-Y. Choi, S. Chattarji, S. Tonegawa, Inhibition of p21-activated kinase rescues symptoms of fragile X syndrome in mice. *Proc. Natl. Acad. Sci. U.S.A.* **104**, 11489–11494 (2007).
71. B. M. Dolan, S. G. Duron, D. A. Campbell, B. Vollrath, B. S. S. Rao, H.-Y. Ko, G. G. Lin, A. Govindarajan, S.-Y. Choi, S. Tonegawa, Rescue of fragile X syndrome phenotypes in *Fmr1* KO mice by the small-molecule PAK inhibitor FRAX486. *Proc. Natl. Acad. Sci. U.S.A.* **110**, 5671–5676 (2013).
72. S. De Rubeis, E. Pasciuto, K. W. Li, E. Fernández, D. Di Marino, A. Buzzi, L. E. Ostroff, E. Klann, F. J. T. Zwartkruis, N. H. Komiyama, S. G. N. Grant, C. Poujol, D. Choquet, T. Achsel, D. Posthuma, A. B. Smit, C. Bagni, CYFIP1 coordinates mRNA translation and cytoskeleton remodeling to ensure proper dendritic spine formation. *Neuron* **79**, 1169–1182 (2013).
73. D. Di Marino, G. Chillemi, S. De Rubeis, A. Tramontano, T. Achsel, C. Bagni, MD and docking studies reveal that the functional switch of CYFIP1 is mediated by a butterfly-like motion. *J. Chem. Theory Comput.* **11**, 3401–3410 (2015).
74. P. Billuart, J. Chelly, From fragile X mental retardation protein to Rac1 GTPase: New insights from fly CYFIP. *Neuron* **38**, 843–845 (2003).
75. C. A. Hoeffer, K. K. Cowansage, E. C. Arnold, J. L. Banko, N. J. Moerke, R. Rodriguez, E. K. Schmidt, E. Klosi, M. Chorev, R. E. Lloyd, P. Pierre, G. Wagner, J. E. LeDoux, E. Klann, Inhibition of the interactions between eukaryotic initiation factors 4E and 4G impairs long-term associative memory consolidation but not reconsolidation. *Proc. Natl. Acad. Sci. U.S.A.* **108**, 3383–3388 (2011).
76. N. J. Moerke, H. Aktas, H. Chen, S. Cantel, M. Y. Reibarkh, A. Fahmy, J. D. Gross, A. Degterev, J. Yuan, M. Chorev, J. A. Halperin, G. Wagner, Small-molecule inhibition of the interaction between the translation initiation factors eIF4E and eIF4G. *Cell* **128**, 257–267 (2007).
77. B. D. Eadie, J. Cushman, T. S. Kannangara, M. S. Fanselow, B. R. Christie, NMDA receptor hypofunction in the dentate gyrus and impaired context discrimination in adult *Fmr1* knockout mice. *Hippocampus* **22**, 241–254 (2012).
78. B. D. Auerbach, E. K. Osterweil, M. F. Bear, Mutations causing syndromic autism define an axis of synaptic pathophysiology. *Nature* **480**, 63–68 (2011).
79. P. W. Frankland, V. Cestari, R. K. Filipkowski, R. J. McDonald, A. J. Silva, The dorsal hippocampus is essential for context discrimination but not for contextual conditioning. *Behav. Neurosci.* **112**, 863–874 (1998).
80. M. S. Fanselow, M. P. Baacke, Conditioned fear-induced opiate analgesia on the formalin test: Evidence for two aversive motivational systems. *Learn. Motiv.* **13**, 200–221 (1982).
81. T. N. Huynh, E. Santini, E. Klann, Requirement of mammalian target of rapamycin complex 1 downstream effectors in cued fear memory reconsolidation and its persistence. *J. Neurosci.* **34**, 9034–9039 (2014).
82. L. Hou, M. D. Antion, D. Hu, C. M. Spencer, R. Paylor, E. Klann, Dynamic translational and proteasomal regulation of fragile X mental retardation protein controls mGluR-dependent long-term depression. *Neuron* **51**, 441–454 (2006).
83. E. D. Nosyreva, K. M. Huber, Metabotropic receptor-dependent long-term depression persists in the absence of protein synthesis in the mouse model of fragile X syndrome. *J. Neurophysiol.* **95**, 3291–3295 (2006).
84. S. H. Fatemi, T. D. Folsom, R. E. Kneeland, M. K. Yousefi, S. B. Liesch, P. D. Thuras, Impairment of fragile X mental retardation protein-metabotropic glutamate receptor 5 signaling and its downstream cognates ras-related C3 botulinum toxin substrate 1, amyloid beta A4 precursor protein, striatal-enriched protein tyrosine phosphatase, and homer 1, in autism: A postmortem study in cerebellar vermis and superior frontal cortex. *Mol. Autism* **4**, 21 (2013).
85. S. J. Heasman, A. J. Ridley, Mammalian Rho GTPases: New insights into their functions from in vivo studies. *Nat. Rev. Mol. Cell Biol.* **9**, 690–701 (2008).
86. B. J. Agnew, L. S. Minamide, J. R. Bamburg, Reactivation of phosphorylated actin depolymerizing factor and identification of the regulatory site. *J. Biol. Chem.* **270**, 17582–17587 (1995).
87. K. Moriyama, K. Iida, I. Yahara, Phosphorylation of Ser-3 of cofilin regulates its essential function on actin. *Genes Cells* **1**, 73–86 (1996).
88. J. A. Ronesi, K. M. Huber, Homer interactions are necessary for metabotropic glutamate receptor-induced long-term depression and translational activation. *J. Neurosci.* **28**, 543–547 (2008).
89. E. Klann, T. E. Dever, Biochemical mechanisms for translational regulation in synaptic plasticity. *Nat. Rev. Neurosci.* **5**, 931–942 (2004).
90. M. C. Mendoza, E. E. Er, J. Blenis, The Ras-ERK and PI3K-mTOR pathways: Cross-talk and compensation. *Trends Biochem. Sci.* **36**, 320–328 (2011).
91. M. Costa-Mattioli, W. S. Sossin, E. Klann, N. Sonenberg, Translational control of long-lasting synaptic plasticity and memory. *Neuron* **61**, 10–26 (2009).

92. T. N. Huynh, M. Shah, S. Y. Koo, K. S. Faraud, E. Santini, E. Klann, eIF4E/*Fmr1* double mutant mice display cognitive impairment in addition to ASD-like behaviors. *Neurobiol. Dis.* **83**, 67–74 (2015).
93. E. Santini, K. L. Turner, A. B. Ramaraj, M. P. Murphy, E. Klann, H. Kaphzan, Mitochondrial superoxide contributes to hippocampal synaptic dysfunction and memory deficits in Angelman syndrome model mice. *J. Neurosci.* **35**, 16213–16220 (2015).
94. H. Kaphzan, S. A. Buffington, A. B. Ramaraj, J. B. Lingrel, M. N. Rasband, E. Santini, E. Klann, Genetic reduction of the α1 subunit of Na/K-ATPase corrects multiple hippocampal phenotypes in Angelman syndrome. *Cell Rep.* **4**, 405–412 (2013).
95. I. Chévere-Torres, H. Kaphzan, A. Bhattacharya, A. Kang, J. M. Maki, M. J. Gambello, J. L. Arbiser, E. Santini, E. Klann, Metabotropic glutamate receptor-dependent long-term depression is impaired due to elevated ERK signaling in the ΔRG mouse model of tuberous sclerosis complex. *Neurobiol. Dis.* **45**, 1101–1110 (2012).
96. H. Hou, A. E. Chávez, C.-C. Wang, H. Yang, H. Gu, B. A. Siddoway, B. J. Hall, P. E. Castillo, H. Xia, The Rac1 inhibitor NSC23766 suppresses CREB signaling by targeting NMDA receptor function. *J. Neurosci.* **34**, 14006–14012 (2014).

Acknowledgments: We thank H. Kaphzan for technical help with the electrophysiology recordings. We also thank F. S. Lee and D. Jing for assistance with Golgi staining. We are grateful to M. Donohue for assistance with mouse breeding. **Funding:** This research was supported by NIH grants NS087112 (to E.S.) and NS034007, NS047384, and HD08201 (to E.K.); Department of Defense Congressionally Directed Medical Research Programs award W81XWH-15-1-0360 (to E.K. and C.B.); and The Queen Elisabeth Medical Foundation Belgium (FMRE), Associazione Italiana Sindrome X Fragile, Telethon GGP15257, and Fonds Wetenschappelijk Onderzoek G.0705.11 (to C.B.). **Author contributions:** E.S., T.N.H., F.L., S.Y.K., E.M., and L.D. performed the experiments; E.S., T.N.H., and F.L. collected and analyzed the data; E.S., T.N.H., F.L., and E.K. designed the experiments; E.S., T.N.H., C.B., and E.K. wrote the manuscript. **Competing interests:** The authors declare that they have no competing interests.

Submitted 2 March 2017
Accepted 18 October 2017
Published 7 November 2017
10.1126/scisignal.aan0665

Citation: E. Santini, T. N. Huynh, F. Longo, S. Y. Koo, E. Mojica, L. D'Andrea, C. Bagni, E. Klann, Reducing eIF4E-eIF4G interactions restores the balance between protein synthesis and actin dynamics in fragile X syndrome model mice. *Sci. Signal.* **10**, eaan0665 (2017).

Science Signaling

Reducing eIF4E-eIF4G interactions restores the balance between protein synthesis and actin dynamics in fragile X syndrome model mice

Emanuela Santini, Thu N. Huynh, Francesco Longo, So Yeon Koo, Edward Mojica, Laura D'Andrea, Claudia Bagni and Eric Klann

Sci. Signal. **10** (504), eaan0665.
DOI: 10.1126/scisignal.aan0665

Finding balance between translation and Rac1 signaling in FXS

Loss of the mRNA translation repressor FMRP in patients with fragile X syndrome (FXS) causes the increased translation of FMRP target transcripts, neurological dysfunction, and intellectual disability. Santini *et al*. found that through its interaction with the scaffolding protein CYFIP1, FMRP sequesters the translation-initiating factor eIF4E and tempers the CYFIP1-mediated facilitation of Rac1-cofilin signaling. Thus, loss of FMRP increased the abundance of eIF4G-bound eIF4E, CYFIP1-Rac1 complexes, and inactivated cofilin, thereby impairing the actin polymerization dynamics necessary for synaptic plasticity and learning. The compound 4EGI-1, which inhibits the formation of eIF4E-mediated translational machinery, reduced protein synthesis and restored a balance with actin dynamics, as well as improved hippocampal synaptic function and dendritic morphology and learning behaviors in FXS model mice. Thus, inhibiting eIF4E-mediated protein synthesis may be therapeutic in FXS patients.